

## RR Lyrae Variables in M33. I. Evidence For a Field Halo Population

Ata Sarajedini and M. K. Barker

*Department of Astronomy, University of Florida, Gainesville, FL 32611*

Doug Geisler

*Grupo de Astronomia, Departamento de Fisica, Universidad de Concepción, Casilla 160-C,  
Concepción, Chile*

Paul Harding

*Astronomy Department, Case Western Reserve University, 10900 Euclid Avenue,  
Cleveland, OH 44106*

Robert Schommer<sup>1</sup>

*Cerro Tololo Inter-American Observatory, National Optical Astronomy Observatories,  
Casilla 603, La Serena, Chile*

### ABSTRACT

We present observations of RR Lyrae variables in the Local Group late-type spiral galaxy M33. Using the Advanced Camera for Surveys on the Hubble Space Telescope, we have identified 64 ab-type RR Lyraes in M33. We have estimated reddenings for these stars based on their minimum light  $V-I$  colors and metallicities based on their periods. From the distributions of these properties, we conclude that the RR Lyraes belong to two populations - one associated with the halo of M33 and the other with its disk. Given that RR Lyraes are produced by populations older than  $\sim 10$  Gyr, this suggests that not only does the field halo of M33 contain an old component, but so does its disk. This is one of the best pieces of evidence for the existence of a halo field component in M33. Using a relation between RR Lyrae absolute magnitude and metallicity ( $M_V(RR) = 0.23[Fe/H] + 0.93$ ), we estimate a mean distance modulus of  $\langle(m - M)_0\rangle = 24.67 \pm 0.08$  for M33. This places M33 approximately 70 kpc beyond M31 in line-of-sight distance.

*Subject headings:* stars: variables: other – galaxies: stellar content – galaxies: spiral – galaxies: individual (M33)

## 1. Introduction

The class of pulsating variables known as RR Lyraes have properties that make them very useful for a number of astrophysical applications. The range of V-magnitudes they exhibit is fairly narrow and their light curve shapes are distinctive (at least for the RRab types) making them easily identifiable. Once identified, their presence is indicative of a stellar population older than  $\sim 10$  Gyr; they can be used as distance indicators; their minimum-light colors reveal the line-of-sight extinction, and their pulsation properties (e.g. amplitudes and periods) are a reflection of their metallicities.

Given their great utility, it is perhaps surprising that RR Lyraes have seen limited use in the study of the stellar populations of M31 and M33 - the only other spiral galaxies in the Local Group besides the Milky Way. Before the advent of the refurbished Hubble Space Telescope, there was a serious dearth of such studies because the faint magnitude of the RR Lyraes at the distances of M31 and M33 ( $V \sim 26$ ) placed them near the magnitude limit of the largest ground-based telescopes. An additional complication in the case of M33 has to do with its orientation on the sky which means halo stars are projected against the disk leading to crowding and confusion problems.

One of the few ground-based studies focusing on the RR Lyraes in M31 was that of Pritchett & van den Bergh (1987). They observed 30 such stars in the halo of M31 using the CFH 3.6m telescope and an early generation RCA CCD. They found a distance for M31 of  $(m - M)_0 = 24.34 \pm 0.15$  based on the mean magnitude of the RR Lyraes. This is slightly closer but still consistent with the (generally accepted) value of  $(m - M)_0 = 24.47 \pm 0.03$ , which represents the weighted mean of seven different recent determinations (Rich et al. 2005).

Ground-based observations of RR Lyraes in M33 were presented by Pritchett (1988). He describes *preliminary* results based on 7 of the best candidate RR Lyraes and computes a distance of  $(m - M)_0 = 24.45 \pm 0.2$ . To put this number in perspective, we note that Galletti, Bellazzini, & Ferraro (2004) have collected distance estimates to M33 using a variety of techniques. The Pritchett (1988) value is on the low side of these various distances. However, the results of Pritchett (1988) remain preliminary and unpublished in the refereed literature.

---

<sup>1</sup>deceased

With the advent of the Hubble Space Telescope (HST), the study of HB stars, and in particular RR Lyraes, in M31 and M33 has become much more tractable. The higher spatial resolution of HST has made it possible to reliably photometer stars in the densest regions of these galaxies (e.g. the bulge of M31, Sarajedini & Jablonka 2005) as well as to magnitudes fainter than the main sequence turnoff in M31 (Brown et al. 2003). The time coverage available from the latter set of observations was exploited by Brown et al. (2004) to study 55 RR Lyraes in a  $\sim 11$  square arcmin region in the halo of M31.

In contrast to M31, there is a paucity of RR Lyrae studies of M33, both from the ground and from space. As a result, we herein describe the results of such a study, which was originally aimed at obtaining deep photometry of two star clusters in M33. As such, although the data are not ideal for an RR Lyrae search, they represent the first space-based study of RR Lyraes in M33 and provide important information about this population. Sections 2 and 3 describe the observations and reductions, respectively. The characterization of the variable stars is also described in Sec. 3. Information that the RR Lyraes provide about the reddening to M33, the metallicity distribution, and the distance of M33 are all discussed in Sec. 4. We discuss our results in Sec. 5. Finally, the conclusions are given in Sec. 6.

## 2. Observations

The images used in the present study were obtained with HST using the Advanced Camera for Surveys instrument (ACS) as part of our GO-9873 program. As shown in Table 1 and Fig. 1, two fields were observed in M33 - one in the vicinity of the star cluster M9 and the other including the clusters U49 and H10. Each exposure indicated in Table 1 was CR-SPLIT resulting in a total of 24 images for each field, 8 in the F606W filter and 16 in the F814W filter. A box-shaped dither pattern was applied with offsets of  $\sim 0.25''$  between each CR-SPLIT exposure. The temporal coverage of each field is  $\sim 2.2$  days.

## 3. Reductions

### 3.1. Construction of Point Spread Functions

The program frames of M33 are extremely crowded making the construction of point spread functions (PSFs) for use in crowded-field photometry quite challenging. In order to more easily construct high S/N PSFs, we have relied on archival images of the globular cluster 47 Tuc obtained as part of three ACS programs: 9656 (PI: De Marchi), 10048 (PI:

Mack), and 10375 (PI: Mack). These are relatively uncrowded fields located  $\sim 6.7$  arcmin from the center of 47 Tuc; thirteen such images are available in the F606W filter and the same number in F814W.

Each WFC1 and WFC2 FLT image was multiplied by the corresponding geometric correction frame and used to generate a PSF via the following procedure. We used the DAOPHOT/ALLSTAR suite of software (Stetson 1987) to find stars on each image and produce small-aperture photometry for them. We then picked 1000 candidate PSF stars. After deleting those with bad pixels nearby, we subtracted the neighboring stars surrounding these PSF stars. The resultant list of between 500 and 700 stars was used to produce a PSF for each of the 13 images in each filter. The shape of the PSF was made to vary quadratically with position on the frame. For each independently derived PSF, the ADDSTAR task in DAOPHOT was used to place 3,240 faint stars on a zero image using the same fixed grid pattern (40 x 81 stars). The resultant 'stack' of 3,240 stars composed of 13 separate and independent PSFs was used to produce a single high S/N PSF for F606W and F814W.

### 3.2. Photometry of Program Frames

Each of the program FLT images was multiplied by the corresponding geometric correction image; the bad pixel masks (i.e. data quality files) were applied and the resultant frames of each ACS chip (WFC1 and WFC2) were photometered with the DAOPHOT/ALLSTAR/ALLFRAME routines (Stetson 1994). We followed the standard procedure for producing crowded-field photometry using these programs (Sarajedini et al. 2000) except that we employed the PSFs described above instead of deriving PSFs from the frames themselves.

To summarize, the process involves producing a coordinate transformation between all of the frames (24 in this case). This transformation is used to produce a median combined image using all of the frames, which is then run through ALLSTAR/FIND/PHOTOMETRY three times to produce a master coordinate list of detected stellar profiles. The coordinate transformation along with the master list and the PSFs are inputs to ALLFRAME which yields profile-fitting magnitudes and positions for stars on each of the 24 frames.

Stars appearing on all of the frames (8 in F606W and 16 in F814W) were matched to form mean instrumental magnitudes. These have been standardized using a two step process. First aperture corrections were derived to correct the PSF mags to an aperture size of 7 pixels where the charge transfer efficiency (CTE) corrections of Reiss (2003) were applied. The magnitudes were then corrected to an infinite radius aperture and transformed to V and I using the relations published by Sirianni et al. (2005). They quote magnitude differences

between a 10 pixel radius aperture and infinity (a radius of 5.5 arcsec) for *drizzled* (DRZ) ACS images. However, because we have photometered the FLT images, it is important to be sure that the magnitude differences between a 10 pixel radius aperture and infinity are the same as those measured for DRZ frames. Therefore, using three F606W and three F814W FLT images of 47 Tuc, the same ones used to construct our PSFs, we find mean differences of  $0.019 \pm 0.011$  mag and  $0.031 \pm 0.019$  (Us – Sirianni) between our aperture corrections and those of Sirianni et al. (2005). Because these differences are not statistically significant, we can safely apply the Sirianni et al. values to our photometry. Based on the discussion in Sec. 8.3 of Sirianni et al. (2005), we adopt an error of  $\pm 0.05$  mag in our photometric zeropoint.

### 3.3. Characterization of Variable Stars

In order to study the variable stars most effectively, we used DAOMASTER to match the stars with measurements on all 24 frames. Stars with frame-to-frame standard deviations greater than 0.2 mag were selected as candidate variable stars for further study. This resulted in  $\sim 400$  candidates in each WFC chip. For comparison, the typical frame-to-frame standard deviation for non-variables stars at the same magnitude as the RR Lyraes is  $\sim 0.08$  mag. The time-series photometry for these stars was then inspected by eye to gauge the quality of the variation. Those light curves deemed to be of sufficiently high quality were analyzed further via the template-light-curve fitting procedure described by Layden & Sarajedini (2000; Pritzl et al. 2002; Mackey & Gilmore 2003). The code written by Andy Layden and available from his web page <sup>2</sup> uses 10 template light curves (6 RRab type variables, 2 RRc types, an eclipsing binary, and an algol binary). It searches over a given period range and calculates the  $\chi^2$  difference between the template and the data. The period that yields the minimum  $\chi^2$  with a given light curve is then fit to that light curve to determine the properties of the variable. For the purposes of the present paper, we are only concerned with the RR Lyrae-type variables. Because the light curves are better sampled in the I-band, the analysis was initially performed on these magnitudes using the V-band data to help constrain the phase. Once an acceptable period and phase were determined from the I-band data, these were used to fit the light curve templates to the V-band observations. In one case, the V-band data do not provide sufficient phase coverage for such a fit (U49-WFC1-131455). Based on our experience with the application of the above-mentioned technique to the observed data points, we estimate an error of  $\pm 0.01$  day in the derived periods. That is to say, most of the time a change of  $\pm 0.01$  day in the optimum period would yield a phased light curve of similar quality, but a change of  $\pm 0.02$  day would frequently yield a light curve of significantly worse

---

<sup>2</sup><http://physics.bgsu.edu/~layden/ASTRO/DATA/EXPORT/progs.htm>

quality. The error is dominated by the particular time sequence of the observations; thus, it is the same for all of the RR Lyrae stars. It should be noted that we checked and re-checked the period determinations of all the RR Lyraes to be certain of their robustness. Given the quality of our data, we are confident that we have derived the best periods possible.

#### 4. Results

The procedure described above yielded 72 RR Lyrae variables in the two ACS fields considered here. Of these, the vast majority (64) are of the RRab type. Table 2 gives the relevant information for each variable. These include the Right Ascension, Declination, intensity weighted mean V and I magnitudes, magnitude weighted mean V–I color, the period in days, the I-band amplitude, and the type of RR Lyrae. Figures 2 through 11 show the light curves of the variables discovered in the present study designated by the field (M9 or U49) and CCD chip (WFC1 or WFC2) in which they are found. It is clear from the light curves that, in some cases, the V-band amplitudes are especially problematic. These should generally be  $\sim 1.6$  times greater than their I-band counterparts (Liu & Janes 1990, Table 6). This is not the case for a number of RR Lyraes in our sample principally because the phase coverage is not sufficient in the V-band.

Figure 12 illustrates the location of the RR Lyraes in the  $(V, V - I)$  color-magnitude diagram (CMD) along with the photometry for the WFC1 chip of the M9 field as a reference. We see that most of the RR Lyraes are located where we expect to see such stars. There is a clear dispersion in their locations in the direction of higher reddening/extinction in the CMD. This is our first indication that not all of the RR Lyraes are located on the near side of M33.

The blue edge of the RR Lyrae instability strip has a color of  $(V - I)_0 = 0.28 \pm 0.02$  (Mackey & Gilmore 2003), which given the line-of-sight reddening toward M33 of  $E(V - I) = 0.06 \pm 0.02$  (Sarajedini et al. 2000), translates to  $(V - I) = 0.34$ . Thus, we expect no RR Lyrae stars bluer than this color, yet Fig. 12 shows 4 stars (M9-WFC2-109239, -112403; U49-WFC1-72044, -88219) that are significantly bluer than  $(V - I) = 0.34$ . The latter two stars are c-type RR Lyraes, which are generally bluer than ab-types. From Fig. 11, it appears that the color of M9-WFC2-109239 is indeed close to zero. In the case of M9-WFC2-112403, the V-band amplitude is underestimated, which could contribute to an overestimate in its inferred V magnitude, thus making the color too blue. Another star in an anomalous location in the CMD is M9-WFC1-21307 located at  $V \sim 24.6$  and  $(V - I) \sim 0.33$ . Again, the light curve appears to be normal, but the magnitude of the variable is too bright by  $\sim 0.5$  mag to be in the canonical RR Lyrae region. This is also the only RR Lyrae in our sample that is located

in the vicinity of a star cluster - that being M9. We suspect the lack of RR Lyrae stars in these clusters is due to their extreme crowding as well as the possibility (Sarajedini et al. 2000) that they are younger than  $\sim 10$  Gyr.

Figure 13 shows the period-amplitude diagram for the RR Lyrae variables. The open circles are the ab-type variables, and the filled circles are those that exhibit sinusoidal light curves indicative of being c-type RR Lyraes. The solid lines are the loci of ab-type RR Lyraes in Oosterhoff I (left) and II (right) globular clusters taken from Clement (2000). The V-band amplitudes ( $Amp_V$ ) of Clement (2000) are converted to I-band values ( $Amp_I$ ) using  $Amp_V = 1.6Amp_I$  determined from Table 6 of Liu & Janes (1990).

A close inspection of Fig. 13 suggests that 5 of the putative c-type RR Lyraes (U49-WFC1-72044, -88219, -102459, -109540, M9-WFC1-60843) occupy a region that is representative of ab-type RR Lyraes. This suggests that these stars are either misclassified ab-type RR Lyraes or that they are an entirely different type of pulsating variable. In addition, c-type variable U49-WFC1-95229 has a period ( $\text{Log } P \sim -0.6$ ) that is much shorter than any of the RR Lyraes probably indicating that it is not an RR Lyrae at all. Because of the ambiguity with regard to the nature of the c-type variables, we will focus only on the RRab variables in the subsequent analysis.

Figure 14 illustrates the period distribution for the RRab type variables. This is compared with RRab stars in the M31 halo (dashed line) from Brown et al. (2004) and in the Galactic globular cluster M3 (dotted line), which is classified as Oosterhoff I (Clement 2000; Brown et al. 2004). The M33 histogram exhibits a primary peak at  $\text{Log } P \sim -0.27$  corresponding to a period of 0.54 days, which is consistent with the mean of 0.55 days characteristic of Oosterhoff I clusters like M3. This is also apparent in the period-amplitude diagram (Fig. 13). The M31 distribution shares a peak with the RR Lyraes in M3, but exhibits a tail to longer periods.

Unlike M31 and M3, the RRab star distribution in M33 exhibits an additional portion that extends to periods as short as  $\sim 0.3$ d. Dividing the RRab sample at 0.44d ( $\text{Log } P = -0.36$ ), we find that 38% of the RRab stars have periods shorter than this value. In contrast, this percentage is only  $\sim 17\%$  among the solar neighborhood RR Lyraes represented in the Northern Sky Variability Survey (Kinemuchi et al. 2005). As we will see in Sec. 4.2, because period and metallicity are correlated for RRab stars, these short period RR Lyraes are most likely an old metal-rich component in the disk of M33. These would necessarily not be seen in a globular cluster like M3 nor the halo of M31.

#### 4.1. RR Lyrae Reddenings

The minimum light color of RRab stars can be used to estimate their line-of-sight reddenings. This is based on a concept originally developed by Sturch (1966), expanded on by Mateo et al. (1995), and most-recently refined by Guldenschuh et al. (2005). The latter work concludes that the intrinsic minimum light color of RRab variables is  $(V-I)_{0,min} = 0.58 \pm 0.02$  with very little dependence on period or metallicity for periods between 0.39d and 0.7d and metallicities in the range  $-3 \lesssim [Fe/H] \lesssim 0$ .

Of the 64 RRab types in our M33 dataset, we were able to fit V-band light curves to all of them except U49-WFC1-131455, which does not possess adequate phase coverage in the V-band. From these light curves, we determine the minimum-light color and use it to calculate the line-of-sight foreground reddening for each RRab star. The distribution of these reddenings is shown by the binned histogram in Fig. 15. For reference, note that the line-of-sight reddening to M33 is  $E(V-I) = 0.06 \pm 0.02$  (Sarajedini et al. 2000). Therefore, we see stars on the near side of M33, reddened only by dust in the Milky Way ( $E(V-I) < 0.1$ ), that are likely to be members of the M33 halo population. We also see RR Lyraes that are reddened by an amount that is in excess of the line-of-sight value suggesting that they are either in the disk of M33 or halo field stars on the far side. The large range of reddening illustrated in Fig. 15 is supported by the presence of a sloping red clump (RC) in the CMD of Fig. 12, wherein the RC slope is consistent with the reddening vector. The reddening range is also consistent with and therefore supported by the results of Boissier et al. (2004) and Massey et al. (1985).

There are 18 stars in Fig. 15 that have negative reddenings, which is clearly unphysical. However, the overall distribution is strongly peaked around zero. Inspection of their light curves shows no clear pattern that would explain this behavior, but, since the reddening distribution is not symmetric around zero, the negative portion of the distribution can be interpreted in terms of the errors in our analysis. Fitting a Gaussian function (dotted lines in Fig. 15) to the negative portion yields  $\sigma = 0.16$  mag in  $E(V-I)$ , while a similar fit to the positive values gives  $\sigma = 0.34$  mag. Subtracting these in quadrature provides a measure of the extinction in the disk of M33 of  $\sigma = 0.30$  mag in  $E(V-I)$ . Utilizing the Sirianni et al. (2005) relations for extinction in the HST/ACS filters gives a 1- $\sigma$  extinction of  $A_{F606W} = 0.62$  mag and  $A_{F814W} = 0.39$  mag.

To place these results in the context of other galaxies, we look to the paper by Holwerda et al. (2005), who investigate the radial extinction properties of nearby spiral galaxy disks using counts of distant galaxies. Their Fig. 4 presents a plot of I-band extinction ( $A_I$ ) as a function of radial location in the galaxy expressed in terms of  $R_{25}$ , which is half the  $D_{25}$  diameter given in the Third Reference Catalog of Bright Galaxies (RC3). For M33, this  $R_{25}$



radius is 35.4 arcmin while the mean deprojected radius of the RR Lyraes is 13.3 arcmin (both fields are at very similar radial distances). Looking at Fig. 4 of Holwerda et al. (2005) at a radius of  $R/R_{25} = 0.38$ , we see that an extinction value ranging from  $A_{F814W} = 0.39$  mag (1- $\sigma$ ) to  $A_{F814W} = 0.78$  mag (2- $\sigma$ ) is consistent with those of the spiral galaxies in Holwerda et al.’s sample.

## 4.2. Metallicities

A number of authors have studied the relationship between the metal abundance of RRab variables and their pulsation periods (e.g. Sandage 1993; Layden 1995). It is well known that as the metallicity of RRab’s increases, their periods decrease. We can exploit this fact to investigate the metal abundances of the M33 RR Lyraes studied herein.

Using the data of Layden (2005, private communication) for 132 Galactic RR Lyraes in the solar neighborhood, we can establish a relation between period and metal abundance. Figure 16 shows these data along with a best-fit line derived by performing a least-squares fit using  $\text{Log } P$  as the independent variable and then with  $[\text{Fe}/\text{H}]$  as the independent variable and combining the results via the OLS Bisector method (Isobe et al. 1990). We find

$$[\text{Fe}/\text{H}] = -3.43 - 7.82 \text{ Log } P_{ab} \quad \text{rms} = 0.45 \text{ dex.} \quad (1)$$

This compares favorably with  $[\text{Fe}/\text{H}] = -4.34 - 10.87 \text{ Log } \langle P_{ab} \rangle$  determined by Brown et al. (2004) based on the findings of Sandage (1993). Both equations are on the Zinn & West (1984) abundance scale. More importantly, the equation derived herein is valid for a larger range of metallicities ( $-2.5 \lesssim [\text{Fe}/\text{H}] \leq 0.0$ ).

Figure 17 shows the distribution of M33 RRab metallicities computed using this equation. The most dominant feature is a strong peak at  $[\text{Fe}/\text{H}] \sim -1.3$ . In addition, there are RR Lyraes with metallicities greater than the solar value. These correspond to the stars with periods shorter than  $\sim 0.35$  days mentioned above. Since our metallicity calibration does not extend beyond  $[\text{Fe}/\text{H}] \sim 0.0$ , these super-solar abundances should be considered with caution and must therefore receive less weight.

In order to quantitatively assess the significance of the apparent bimodality in the metallicity distribution, we utilize the KMM mixture-modeling algorithm (McLachlan & Basford 1988). This algorithm objectively partitions a dataset into two (or more) components and then assesses the improvement of the two-group fit to the one-group fit using the likelihood ratio test statistic (see Ashman, Bird & Zepf 1994 for a discussion of this algorithm in the

context of astronomical applications). We find that the KMM algorithm rejects the unimodal hypothesis in favor of the bimodal one at a confidence level of  $> 99.9\%$ , irrespective of whether the stars with supra-solar metallicities are assigned their nominal values or are simply assigned a metallicity of 0. This confirms the reality of the two metallicity populations that appear visually.

Attributing the root-mean-square residual of the fit shown in Fig. 16 (0.45 dex) as the error in each individual abundance, we can construct a generalized histogram of the metallicity values. This is shown as the dashed curve in Fig. 17. For reference, we note that at the mean deprojected galactocentric distance of the RR Lyraes ( $3.36 \pm 0.05$  kpc), the metal abundance of the red giant branch stars in the M33 disk is  $[Fe/H] = -0.72 \pm 0.03$ ; this is based on the relation published by Kim et al. (2002) of  $[Fe/H] = -0.05(\pm 0.01)R_{deproj}(kpc) - 0.55(\pm 0.03)$ . In addition, the mean metallicity of halo globular clusters in M33 is  $[Fe/H] = -1.27 \pm 0.11$  (Sarajedini et al. 2000). The solid line in Fig. 17 shows two Gaussian distributions, one with a peak at  $[Fe/H] = -0.7$  (disk) and the other at  $[Fe/H] = -1.3$  (halo) fitted to the generalized histogram (dashed line). The fact that the Gaussian fits are consistent with the observed metallicity distribution of the RR Lyraes suggests that the metal-rich population can be attributed to the disk of M33 while the more metal-poor population belongs to the halo. This confirms what we concluded from the distribution of RR Lyrae reddenings, namely that our RR Lyrae sample is composed of both halo and disk populations.

### 4.3. Distance of M33

As noted in Sec. 1, we can make use of the RR Lyrae stars to determine the distance to M33. We will not use stars with super-solar abundances because our  $\text{Log } P \sim [\text{Fe}/\text{H}]$  calibration is uncertain for these stars. The mean V magnitude of the 43 RRab stars with positive reddening values and metallicities less than solar is  $\langle V(RR) \rangle = 25.92 \pm 0.05$  (ran)  $\pm 0.05$  (sys), where the random error is the standard error of the mean and the systematic error represents the uncertainty in the photometric zeropoint. Applying the reddenings to the apparent magnitudes using  $A_{F606W} = 2.1E(V - I)$  gives a mean intrinsic V magnitude of  $\langle V_0(RR) \rangle = 25.34 \pm 0.07$ , where we have added the random and systematic errors in quadrature.

The next step involves adoption of metallicities for each RR Lyrae star. This has already been discussed above where we presented our equation relating the RR Lyrae's pulsation period with its metal abundance. To calculate the absolute magnitude from the metallicity, we rely upon the relation  $M_V(RR) = 0.23[Fe/H] + 0.93$  derived by Chaboyer (1999). In this case, the mean absolute distance modulus for the 43 RRab stars with positive reddenings

and subsolar metallicities turns out to be  $\langle(m - M)_0\rangle = 24.67 \pm 0.08$ . This value for the distance modulus is in very good agreement with the results of Galleti et al. (2004) who find an average distance of  $\langle(m - M)_0\rangle = 24.69 \pm 0.15$  based on 19 independent estimates.

Since our mean I-band magnitudes are generally better determined than those in the V-band, we can also estimate the distance of M33 using the I-band data. Doing this, we find  $\langle I(RR)\rangle = 25.11 \pm 0.03$  (ran)  $\pm 0.05$  (sys) for the 43 RR Lyraes in our subsample. Applying the reddenings for each individual star yields  $\langle I_0(RR)\rangle = 24.73 \pm 0.06$ . Employing once again the Chaboyer (1999) equation relating RR Lyrae absolute magnitude and metallicity, we find  $\langle M_V(RR)\rangle = 0.67 \pm 0.03$ . Now we need to convert  $M_V(RR)$  to  $M_I(RR)$  using the mean color of the RRab stars in our sample of  $\langle(V - I)_0\rangle = 0.55 \pm 0.02$ . Doing so and recomputing the distance, we arrive at  $\langle(m - M)_0\rangle = 24.61 \pm 0.07$ , which agrees to within the errors with the value determined using the V-band RR Lyrae magnitudes.

One could argue that, from a statistical point of view, the negative reddenings should not be ignored, but rather should be included in the calculation of the distance. In this case, we find  $\langle(m - M)_0\rangle = 24.76 \pm 0.08$  based on the V-band RR Lyrae magnitudes and  $\langle(m - M)_0\rangle = 24.72 \pm 0.07$  from the I-band magnitudes. Again, both of these are consistent with the mean distance modulus from the work of Galleti et al. (2004).

## 5. Discussion

The presence of star clusters in a kinematically hot halo has been recognized for some time in M33. The pioneering work of Schommer et al. (1991) and the more recent results of Chandar et al. (2002) confirm this fact. However, the existence of a field star component to the halo has been an open question for some time. Studies of the halo field in M33 go back to the seminal work of Mould & Kristian (1986, MK86). They present a CMD of a “halo” field located  $\sim 20$  arcmin from M33’s center along the minor axis in the southeast direction. By comparing this diagram with standard giant branches, MK86 concluded that the mean metal abundance of the M33 halo is  $\langle[M/H]\rangle = -2.2 \pm 0.8$ . Such a metal-poor halo abundance is in contrast to the mean metal abundance of halo clusters of  $\langle[Fe/H]\rangle = -1.27 \pm 0.11$  (Sarajedini et al. 2000). This apparent discrepancy was resolved by Tiede, Sarajedini, & Barker (2004) who reobserved the MK86 field and constructed the deepest ground-based CMD of M33 to date. Analysis of these data reveals that the radial metallicity gradient of the MK86 “halo” field precisely matches that of the M33 inner disk suggesting that the MK86 field is dominated by M33 disk stars NOT halo stars. Tiede et al. (2004) identified problems with the color calibration of the MK86 photometry as the source of the differences between the two studies.

The quest to identify the halo field-star population of M33 finally found success in the recent study by Brooks et al. (2004). They constructed a radial stellar density profile out to 1 degree from the center of M33 corresponding to a projected distance of about 16 kpc. The slope of their density profile, which includes red giant branch (RGB) stars with  $20.5 < I < 22.5$ , is relatively shallow ( $-1.46 \pm 0.14$  in the  $\text{Log } \sigma \sim \text{Log } R$  plane), suggesting the presence of a halo population. Interestingly, the peak metallicity of the halo as determined by Brooks et al. (2004) is  $[Fe/H] = -1.24 \pm 0.04$ , which is gratifyingly close to the mean abundance Sarajedini et al. (2000) derive for the halo globular clusters of  $\langle [Fe/H] \rangle = -1.27 \pm 0.11$ .

With the discovery and characterization of RR Lyraes in M33 described herein, we have again shown that the halo field star population of M33 is non-negligible. The peak metal abundance of these putative halo RR Lyraes is consistent with that of the halo globular clusters presented by Sarajedini et al. (2000). In addition, the presence of these RR Lyraes indicates that the halo field stars of M33 possess a significant old population ( $\gtrsim 10$  Gyr), which along with the diversity of HB types seen among the halo globular clusters (Sarajedini et al. 2000), further reinforces the idea that the halo of M33 formed over a time period of 5 to 7 Gyr as first suggested by Sarajedini et al. (1998). This is in stark contrast to the Milky Way halo which is mostly old and formed over only a few Gyr. The presence of old ( $\gtrsim 10$  Gyr), metal-rich RR Lyrae stars presumably in the disk of M33 is also very interesting and deserving of further study.

## 6. Conclusions

We present HST/ACS observations of two fields in the Local Group spiral galaxy M33. The time baseline of our photometry from these observations spans  $\sim 2.2$  days allowing us to identify RR Lyraes in M33 from space-based data for the first time. From the properties of 64 ab-type RR Lyraes, we draw the following conclusions.

- 1) The minimum light colors of these stars provide a means by which to calculate reddenings. The distribution of reddenings suggests the presence of RR Lyraes in the halo and disk of M33.
- 2) The periods of the RR Lyraes provide a means by which to calculate metallicities. The distribution of metallicities also suggests the presence of RR Lyraes in the halo and disk.
- 3) Thus, both the field-halo and disk of M33 possess an old stellar population with an age of  $\gtrsim 10$  Gyr.
- 4) Based on the mean V and I band magnitudes of these stars, along with period-based

metallicities, and the Chaboyer (1993) relation between RR Lyrae metallicity and absolute magnitude, we calculate a mean distance modulus of  $\langle(m - M)_0\rangle = 24.67 \pm 0.08$  placing M33  $\sim 70$  kpc further away than M31.

We are grateful to Andy Layden for providing his suite of software for performing the light curve fitting as well as his useful advice in the area of RR Lyrae properties. A.S. and M.K.B. received support for this work (proposal number GO-9873) from NASA through a grant from the Space Telescope Science Institute which is operated by the Association of Universities for Research in Astronomy, Incorporated, under NASA contract NAS5-26555. D.G. gratefully acknowledges support from the Chilean *Centro de Astrofísica* FONDAF No. 15010003.

## REFERENCES

- Ashman, K.M., Bird, C.M. & Zepf, S.E. 1994, *AJ*, 108, 2348
- Boissier, S., Boselli, A., Buat, V., Donas, J., & Milliard, B. 2004, *A&A*, 424, 465
- Brooks, R. S., Wilson, C. D., & Harris, W. E. 2004, *AJ*, 128, 237
- Brown, T., Ferguson, H. C., Smith, E., Kimble, R. A., Sweigart, A. V., Renzini, A., Rich, R. M., & Vandenberg, D. A. 2003, *ApJ*, 592, L17
- Brown, T. M., Ferguson, H. C., Smith, E., Kimble, R. A., Sweigart, A., V. Renzini, A., & Rich, R. M. 2004, *AJ*, 127, 2738
- Chaboyer, B. 1999, in *Post Hipparcos Cosmic Candles*, edited by A. Heck and F. Caputo (Kluwer: Dordrecht) p.111
- Chandar, R., Bianchi, L., Ford, H. C., & Sarajedini, A. 2002, *ApJ*, 564, 712
- Clement, C. M. 2000, in *IAU Colloq. 176, The Impact of Large Scale Research on Pulsating Star Research*, ed. L. Szabados & D. W. Kurtz (ASP Conf. Ser. 203) (San Francisco:ASP), 266
- Galletti, S., Bellazzini, M., & Ferraro, F. R. 2004, *A&A*, 423, 925
- Guldenschuh, K. et al. 2005, *PASP*, 117, 721
- Holwerda, B. W., Gonzalez, R. A., Allen, R. J., vanderKruit, P. C. 2005, *AJ*, 129, 1396

- Isobe, T., Feigelson, E. D., Akritas, M. G., & Babu, G. J. 1990, *ApJ*, 364, 104
- Kim, M., Kim, E., Lee, M. G., Sarajedini, A., & Geisler, D. 2002, *AJ*, 123, 244
- Kinemuchi, K., Smith, H. A., McKay, T. A., Wozniak, P. R., & ROTSE Collaboration, 2005, *BAAS*, December
- Layden, A. C. 1995, *AJ*, 110, 2312
- Layden, A. C., & Sarajedini, A. 2000, *AJ*, 119, 1760
- Liu, T., & Janes, K. A. 1990, *ApJ*, 354, 273
- Mackey, A. D., & Gilmore, G. F. 2003, *MNRAS*, 345, 747
- Massey, P., Armandroff, T. E., Pyke, R., Patel, K., & Wilson, C. D. 1995, *AJ*, 110, 2715
- Mateo, M., Udalski, A., Szymański, M., Kaluźny, J., Kubiak, M., & Krzemiński, W. 1995, *AJ*, 109, 588
- McLachlan, G.J. & Basford, K.E., 1988, *Mixture Models: Inference and Applications to Clustering* (New York: Marcel Dekker)
- Mould, J. R., & Kristian, J. 1986, *ApJ*, 305, 591 (MK86)
- Pritchett, C. J. 1988, in *The Extragalactic Distance Scale; Proceedings of the ASP 100th Anniversary Symposium (ASP:San Francisco)* p. 59
- Pritchett, C. J., & vandenBergh, S. 1987, *ApJ*, 316, 517
- Pritzl, B. J., Armandroff, T. E., Jacoby, G. H., & DaCosta, G. S. 2002, *AJ*, 124, 1464
- Reiss, A. 2003, *ACS-ISR 2003-09*
- Sandage, A. 1993, *AJ*, 106, 687
- Sarajedini, A., & Jablonka, P. 2005, *AJ*, 130, 1627
- Sarajedini, A., Geisler, D., Schommer, R., & Harding, P. 2000, *AJ*, 120, 2437
- Schommer, R. A., Christian, C. A., Caldwell, N., Bothun, G. D., & Huchra, J. 1991, *AJ*, 101, 873
- Sirianni, M. et al. 2005, *PASP*, 117, 1049
- Stetson, P. B. 1987, *PASP*, 99, 191

Stetson, P. B. 1994, PASP, 106, 250

Sturch, C. 1966, ApJ, 143, 774

Tiede, G. P., Sarajedini, A., & Barker, M. 2004, AJ, 128, 224

Table 1. Observing Log

Field	RA (2000)	Dec	PA V3 <sup>a</sup>	Filter	Exp Time
U49	1h 33m 40s	+30° 47' 59"	316.59	F606W F814W	1 x 2494s, 3 x 2640s 2 x 2494s, 6 x 2640s
M9	1h 34m 30s	+30° 38' 13"	239.45	F606W F814W	1 x 2494s, 3 x 2640s 2 x 2494s, 6 x 2640s

<sup>a</sup>Position angle of V3-axis of HST in degrees.



Table 2. RR Lyrae Properties

Name	RA (2000)	Dec	$\langle V \rangle$	$\langle I \rangle$	$\langle (V - I) \rangle$	Period (days)	Amp. I	Type
U49 - WFC1								
60242	1 33 43.08	30 48 33.3	25.477	24.721	0.825	0.640	0.557	ab
72044	1 33 43.22	30 48 6.2	25.036	24.823	0.202	0.681	0.569	c
83628	1 33 36.99	30 48 5.0	25.371	24.959	0.385	0.329	0.849	ab
88085	1 33 40.72	30 47 46.9	25.406	25.010	0.431	0.336	0.912	ab
88219	1 33 45.58	30 47 55.2	25.113	24.879	0.275	0.501	0.931	c
88263	1 33 41.13	30 47 25.0	25.732	25.035	0.738	0.339	0.836	ab
95931	1 33 42.28	30 48 49.0	25.313	25.093	0.419	0.490	0.701	ab
100315	1 33 34.10	30 47 15.1	26.033	25.055	0.960	0.552	0.705	ab
102459	1 33 39.08	30 48 47.2	25.725	25.122	0.585	0.512	0.691	c
102996	1 33 41.05	30 47 17.6	26.160	25.133	1.084	0.611	0.622	ab
103812	1 33 34.27	30 47 45.6	26.056	25.079	0.970	0.536	0.429	ab
104521	1 33 38.15	30 46 32.9	26.109	25.133	0.964	0.553	0.525	ab
109540	1 33 40.62	30 48 31.0	25.789	25.292	0.466	0.526	0.740	c
114242	1 33 35.91	30 48 5.2	25.994	25.241	0.781	0.405	0.676	ab
116063	1 33 48.45	30 48 39.0	26.142	25.287	0.885	0.537	0.505	ab
116629	1 33 41.52	30 48 59.9	25.994	25.336	0.654	0.377	0.573	ab
119179	1 33 40.11	30 48 22.5	26.191	25.324	0.839	0.429	0.877	ab
120673	1 33 35.50	30 47 23.5	25.866	25.421	0.498	0.417	0.882	ab
121343	1 33 43.27	30 47 26.3	26.255	25.259	1.008	0.570	0.689	ab
131455	1 33 38.28	30 48 3.6	26.667	25.426	1.212	0.600	0.867	ab
132610	1 33 40.72	30 47 37.6	26.386	25.371	1.087	0.546	0.651	ab
132766	1 33 44.53	30 49 22.3	26.438	25.355	1.081	0.333	0.332	c
U49 - WFC2								
61160	1 33 32.58	30 49 35.2	25.794	24.860	0.955	0.595	0.617	ab
65431	1 33 38.14	30 50 19.2	26.075	25.080	0.985	0.530	0.775	ab
66329	1 33 36.15	30 49 19.6	25.712	25.087	0.632	0.592	0.845	ab
68673	1 33 33.46	30 48 35.4	26.359	25.091	1.258	0.536	0.750	ab
76675	1 33 36.07	30 49 36.2	26.010	25.221	0.791	0.520	0.813	ab
77426	1 33 31.66	30 48 57.4	26.064	25.052	0.986	0.498	0.783	ab
85243	1 33 33.22	30 48 3.8	26.196	25.360	0.840	0.560	0.738	ab
95229	1 33 29.96	30 48 21.0	26.275	25.511	0.749	0.250	0.623	c
97246	1 33 31.52	30 48 12.3	26.159	25.596	0.557	0.514	0.587	ab
97903	1 33 37.68	30 49 28.9	26.574	25.431	1.143	0.393	0.489	ab
99949	1 33 35.60	30 50 29.9	26.552	25.546	1.006	0.330	0.374	ab
102256	1 33 38.61	30 49 11.1	26.404	25.507	0.906	0.407	0.608	ab
102530	1 33 39.93	30 49 14.6	26.312	25.696	0.614	0.492	0.272	c
103379	1 33 35.23	30 49 22.4	26.249	25.575	0.798	0.440	0.839	ab
M9 - WFC1								
21307	1 34 30.25	30 38 12.6	24.680	24.347	0.340	0.333	0.679	ab
43952	1 34 25.01	30 39 6.1	25.210	24.759	0.462	0.559	0.657	ab
45819	1 34 30.89	30 39 7.5	25.202	24.809	0.415	0.571	0.747	ab
49806	1 34 27.67	30 39 19.9	25.328	24.804	0.543	0.559	0.754	ab
50684	1 34 29.87	30 38 19.3	25.311	24.815	0.562	0.368	0.664	ab

Table 2—Continued

Name	RA (2000)	Dec	$\langle V \rangle$	$\langle I \rangle$	$\langle (V - I) \rangle$	Period (days)	Amp. I	Type
53358	1 34 28.80	30 38 22.3	25.333	24.940	0.418	0.319	0.538	ab
55610	1 34 33.87	30 38 12.7	25.551	25.001	0.574	0.520	0.751	ab
57000	1 34 33.94	30 37 58.9	25.741	25.004	0.724	0.409	0.838	ab
57039	1 34 31.84	30 37 20.7	25.678	24.990	0.713	0.522	0.822	ab
57707	1 34 28.36	30 37 22.1	25.815	24.913	0.880	0.387	0.766	ab
60843	1 34 31.88	30 37 42.6	25.774	25.050	0.697	0.589	0.697	c
67510	1 34 29.86	30 37 41.8	25.662	25.212	0.518	0.518	0.791	ab
73401	1 34 32.58	30 37 33.0	26.119	25.393	0.726	0.322	0.572	ab
M9 - WFC2								
59370	1 34 20.53	30 38 46.7	25.134	24.740	0.404	0.321	0.616	ab
63575	1 34 19.00	30 37 49.5	25.402	24.996	0.422	0.496	0.902	ab
68851	1 34 20.72	30 36 51.9	25.194	24.865	0.364	0.512	0.738	ab
69612	1 34 20.71	30 36 44.5	25.382	24.859	0.555	0.496	0.564	ab
70023	1 34 22.02	30 38 54.3	25.345	24.907	0.473	0.333	0.837	ab
72301	1 34 24.65	30 36 25.9	25.343	24.861	0.513	0.356	0.601	ab
73898	1 34 19.68	30 37 33.1	25.329	24.832	0.518	0.529	0.736	ab
76410	1 34 19.59	30 37 14.7	25.657	24.824	0.827	0.570	0.698	ab
77532	1 34 22.47	30 37 23.3	25.405	24.896	0.535	0.320	0.744	ab
82703	1 34 25.74	30 37 53.4	25.530	25.007	0.546	0.505	0.739	ab
85311	1 34 26.19	30 37 45.4	25.727	24.848	0.859	0.546	0.818	ab
86029	1 34 22.22	30 37 55.9	25.816	24.893	0.906	0.555	0.701	ab
87001	1 34 23.48	30 38 2.6	25.642	25.060	0.592	0.463	0.711	ab
88677	1 34 24.48	30 35 55.3	25.791	24.901	0.864	0.529	0.749	ab
92546	1 34 26.07	30 36 53.9	25.575	24.944	0.615	0.395	0.771	ab
94025	1 34 20.39	30 37 12.0	25.962	25.015	0.934	0.595	0.644	ab
94890	1 34 22.02	30 37 38.9	25.861	25.077	0.773	0.552	0.696	ab
95126	1 34 28.83	30 36 55.2	25.970	25.004	0.965	0.541	0.701	ab
97250	1 34 29.44	30 36 42.0	25.695	25.247	0.466	0.420	0.875	ab
109239	1 34 22.33	30 37 28.4	25.431	25.356	0.092	0.539	0.524	ab
112403	1 34 23.65	30 37 12.7	25.883	25.607	0.269	0.396	0.479	ab
119403	1 34 20.41	30 38 29.8	26.641	25.388	1.238	0.549	0.796	ab
125762	1 34 23.17	30 36 4.7	26.006	25.532	0.463	0.484	0.554	ab

Fig. 1.— The location of our observed ACS fields overplotted on the DSS-II image of M33. The field is approximately 20 arcmin a side; North is up and east is to the left.

Fig. 2.— Light curves for candidate RR Lyraes in the U49 WFC1 field. The open circles are the I-band data while the filled circles are the V-band.

Fig. 3.— Same as Fig. 2.

Fig. 4.— Same as Fig. 2.

Fig. 5.— Light curves for candidate RR Lyraes in the U49 WFC2 field. The open circles are the I-band data while the filled circles are the V-band.

Fig. 6.— Same as Fig. 5.

Fig. 7.— Light curves for candidate RR Lyraes in the M9 WFC1 field. The open circles are the I-band data while the filled circles are the V-band.

Fig. 8.— Same as Fig. 7.

Fig. 9.— Light curves for candidate RR Lyraes in the M9 WFC2 field. The open circles are the I-band data while the filled circles are the V-band.

Fig. 10.— Same as Fig. 9.

Fig. 11.— Same as Fig. 9.

Fig. 12.— The color-magnitude diagram of the M9-WFC1 field showing the locations of the RR Lyrae stars identified in this paper. The reddening vector for  $E(V-I) = 0.3$  is also shown.

Fig. 13.— The period-amplitude diagram for the RR Lyraes in M33. The open and filled circles are ab-type and c-type variables, respectively. The solid lines are the loci for Oosterhoff I (left) and II (right) globular clusters from Clement (2000). These have been converted from V-band amplitudes to I-band by dividing them by 1.6 as per the results of Liu & Janes (1990).

Fig. 14.— The distribution of periods for the ab-type RR Lyraes in the present work (solid line). Analogous distributions for the M31 halo (Brown et al. 2004) and the globular cluster M3 (Brown et al. 2004) are shown as the dashed and dotted lines, respectively. These have been scaled to have the same number of RR Lyraes as the M33 distribution.

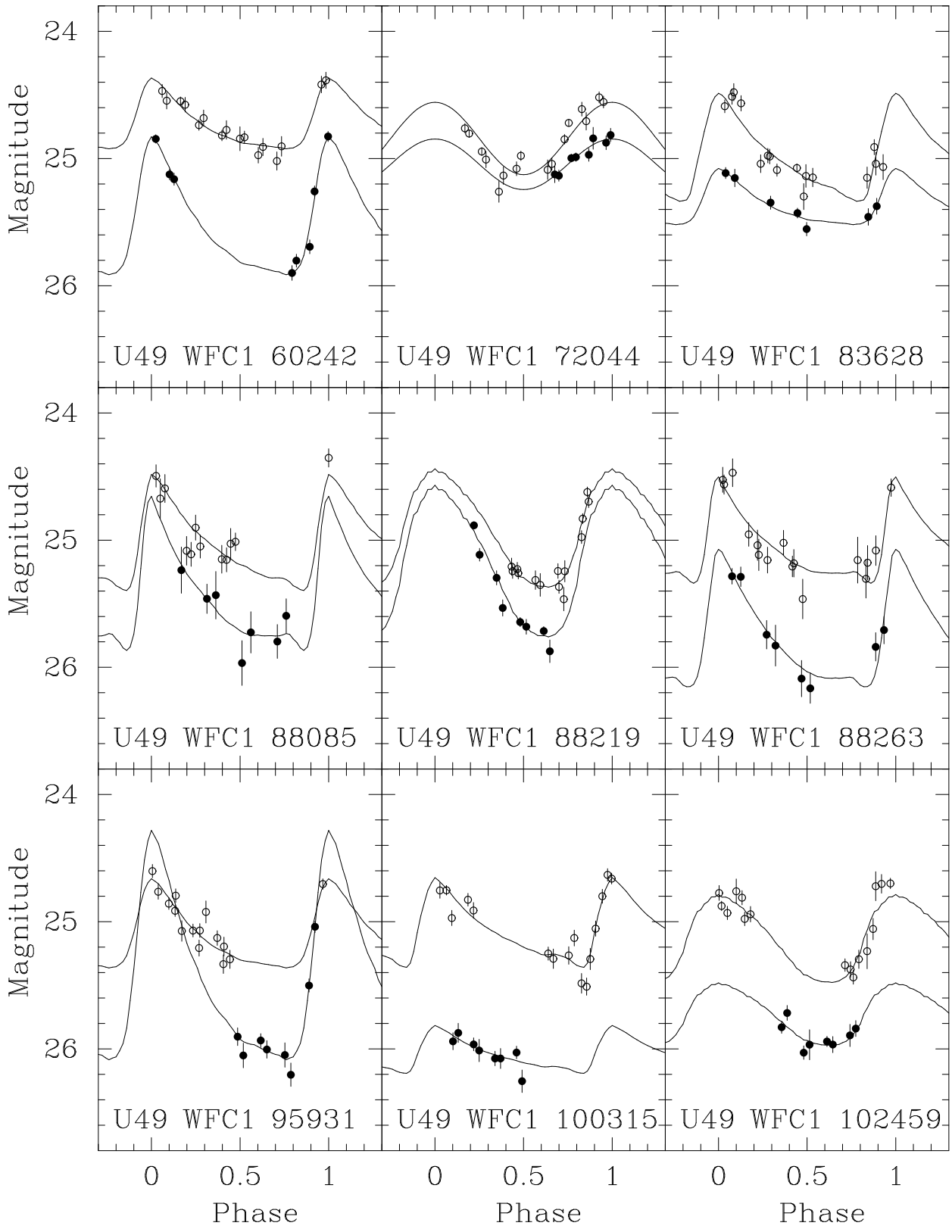
Fig. 15.— The distribution of  $E(V - I)$  reddenings determined for the 63 RRab stars with adequate light curves using the method of Sturch (1966). The dotted lines are Gaussian fits to the negative and positive portions of the reddening distribution.

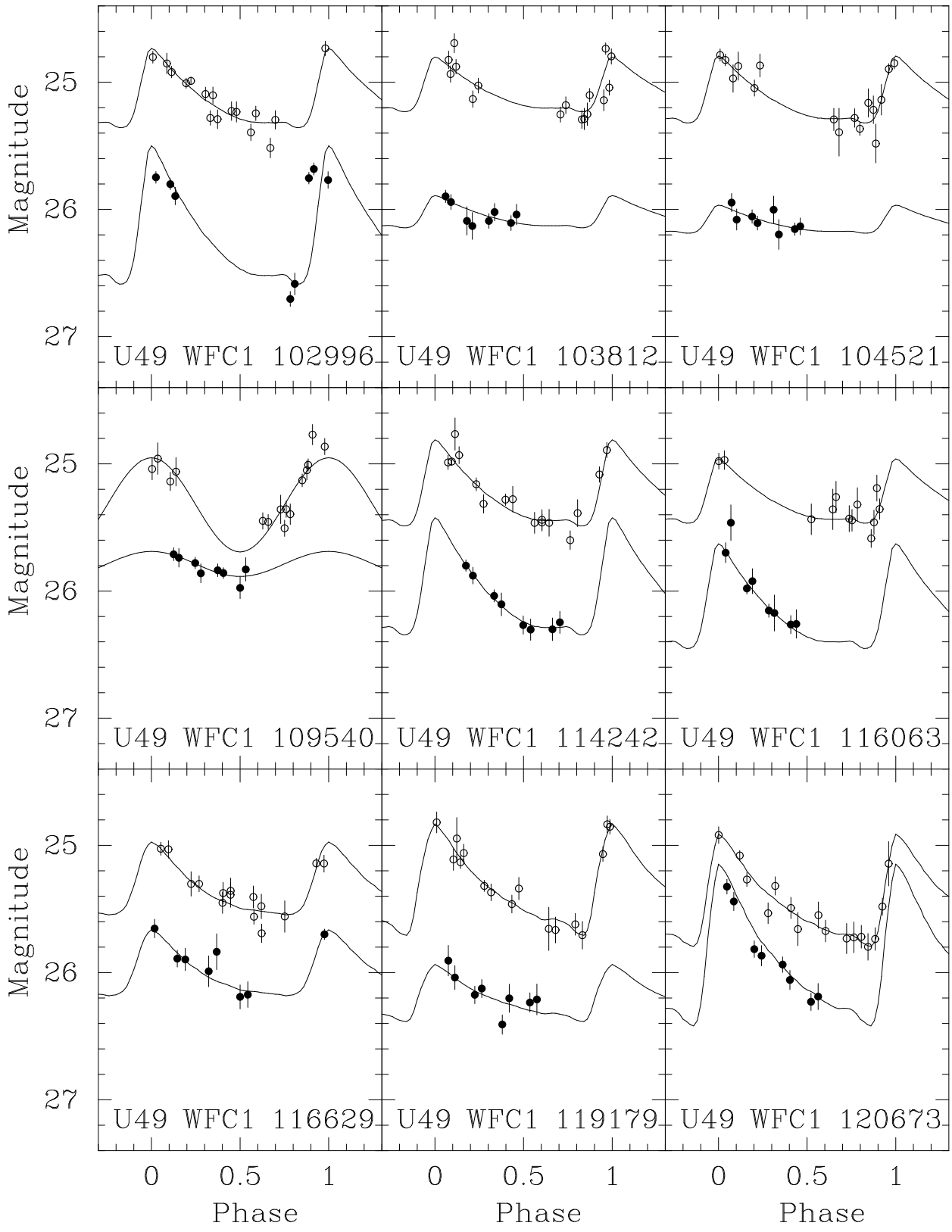
Fig. 16.— A plot of the metal abundance of Galactic RRab stars in the Layden (2005, private communication) database as a function of the logarithm of the period in days (Log P). The dashed line is the best-fit relation determined by performing a least-squares fit using Log P as the independent variable and then with  $[Fe/H]$  as the independent variable and combining the results (see text). The root-mean-square deviation of the points from the fit is 0.45 dex.

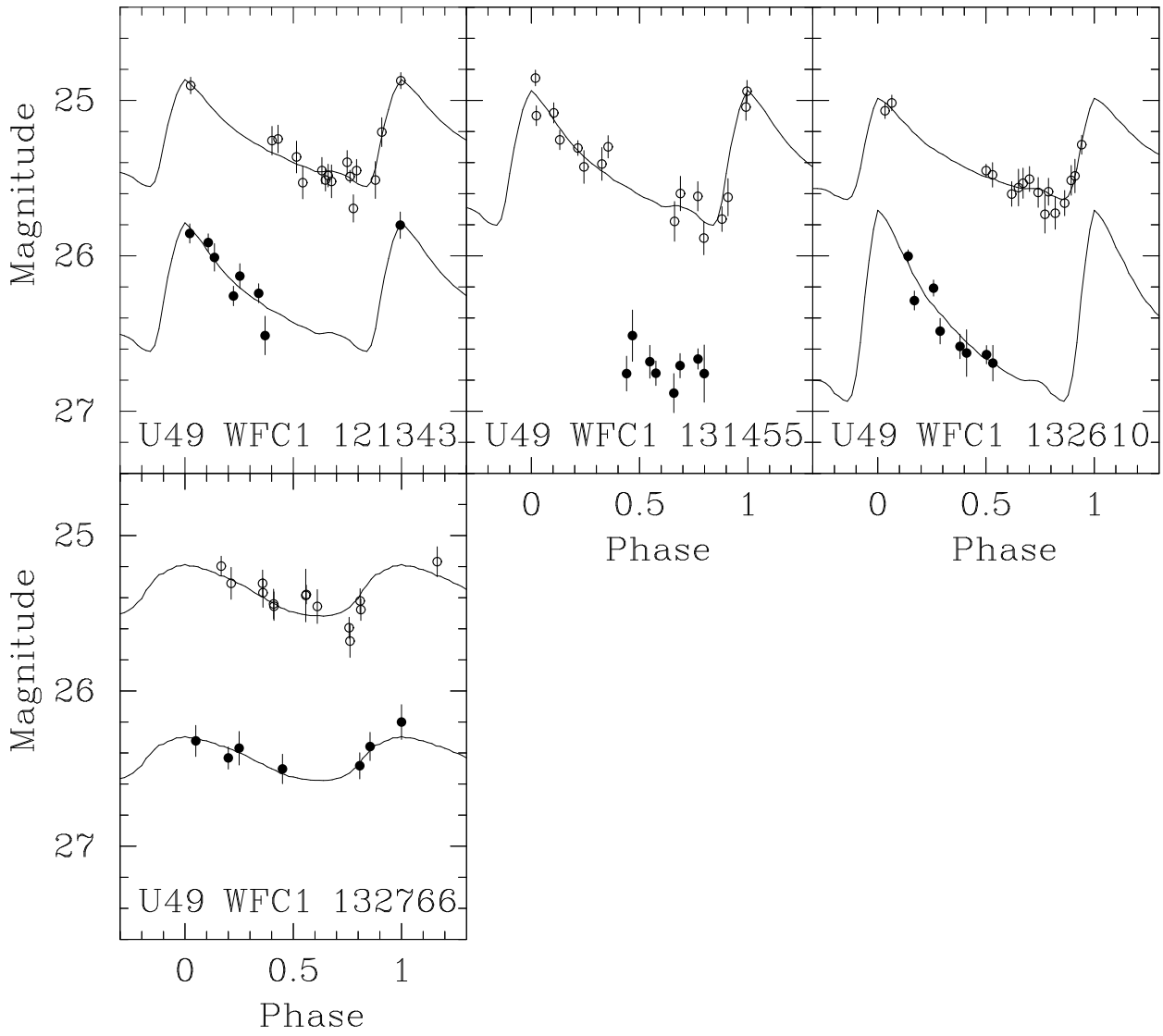
Fig. 17.— The distribution of metallicities determined from the period of each M33 RRab star. The dashed line is the generalized histogram of metallicity values assuming an error of 0.45 dex for each value. The solid line is the sum of two Gaussian distributions, one with a peak at  $[Fe/H] = -1.3$  and the other with a peak at  $[Fe/H] = -0.7$ , fitted to the generalized histogram.

This figure "f1.jpg" is available in "jpg" format from:

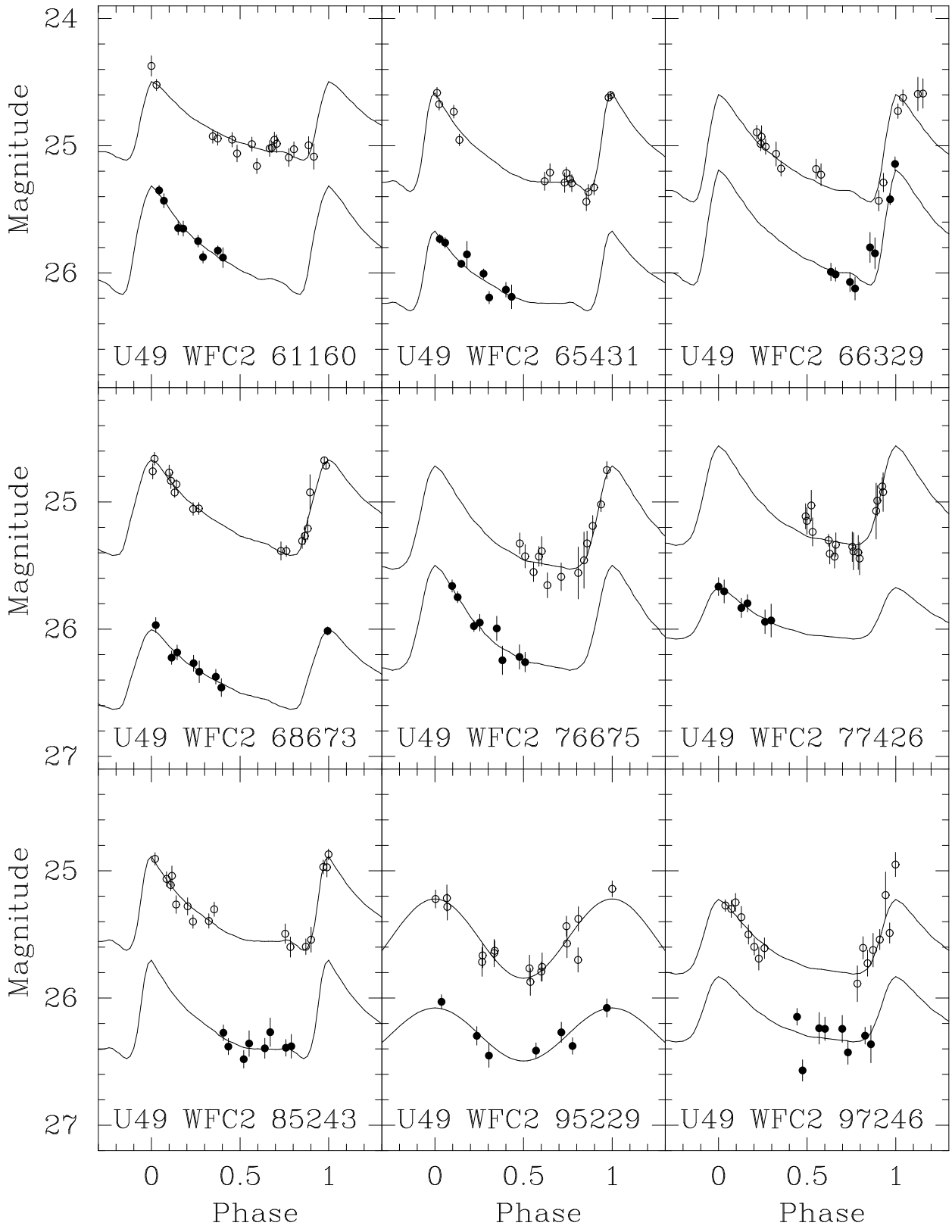
<http://arxiv.org/ps/astro-ph/0605580v1>

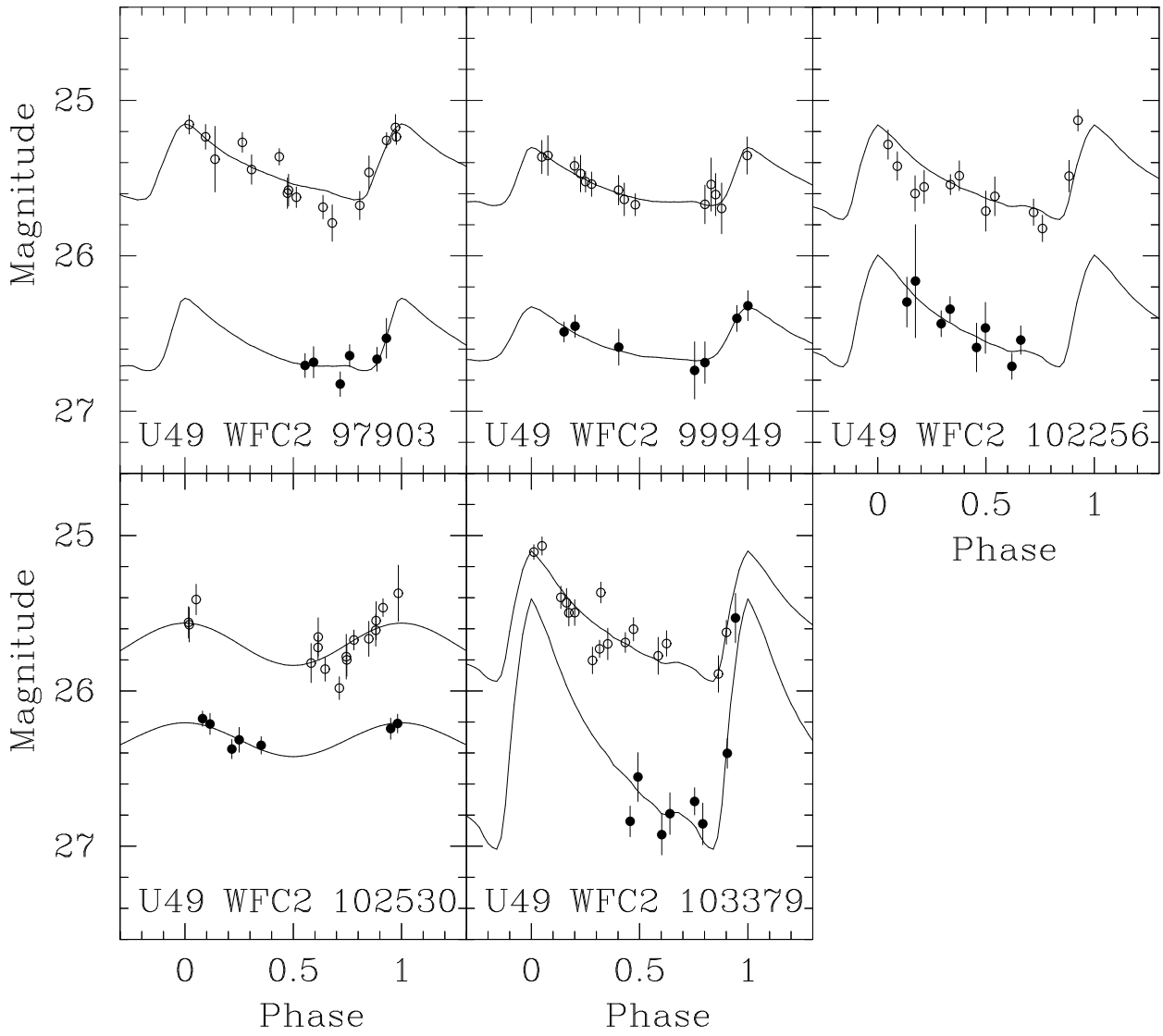


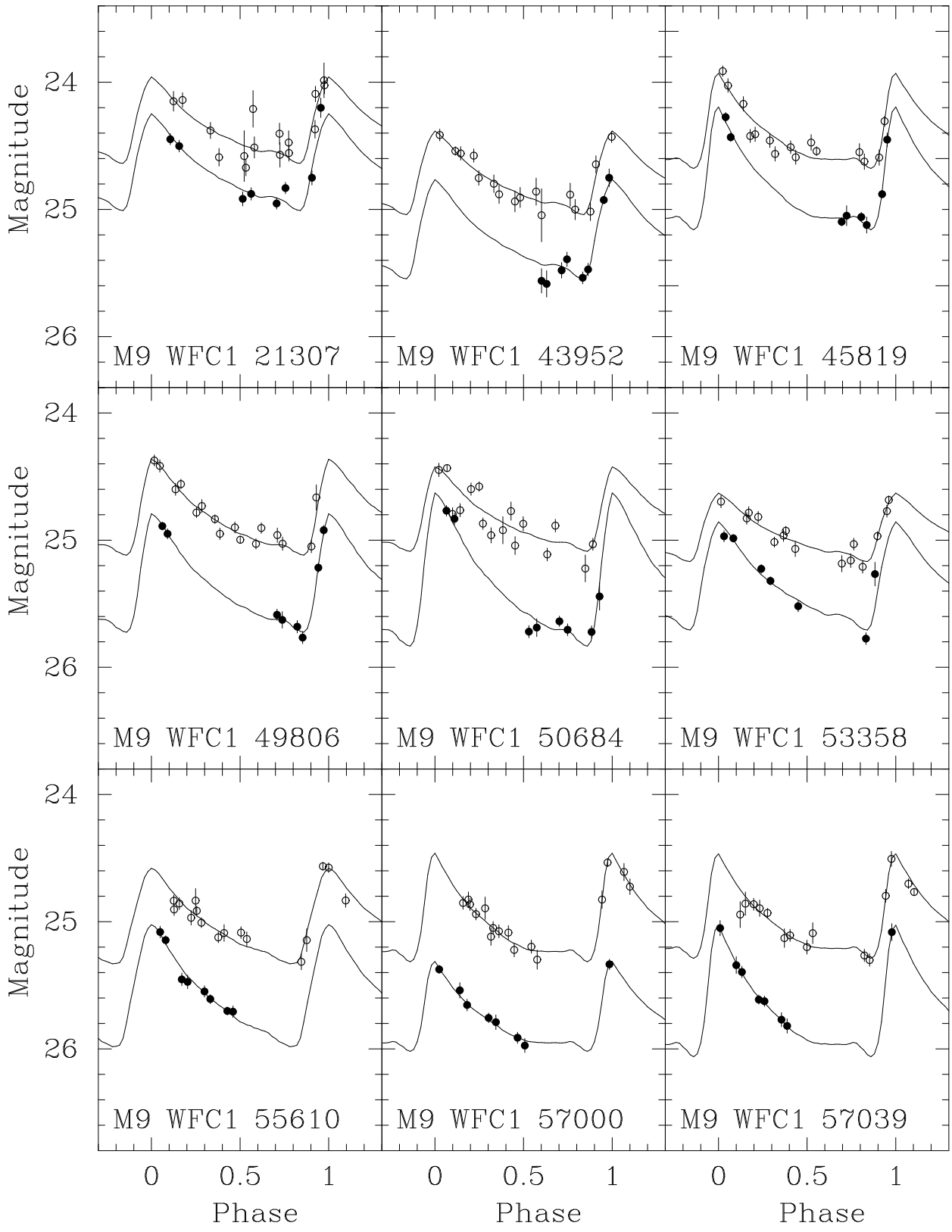


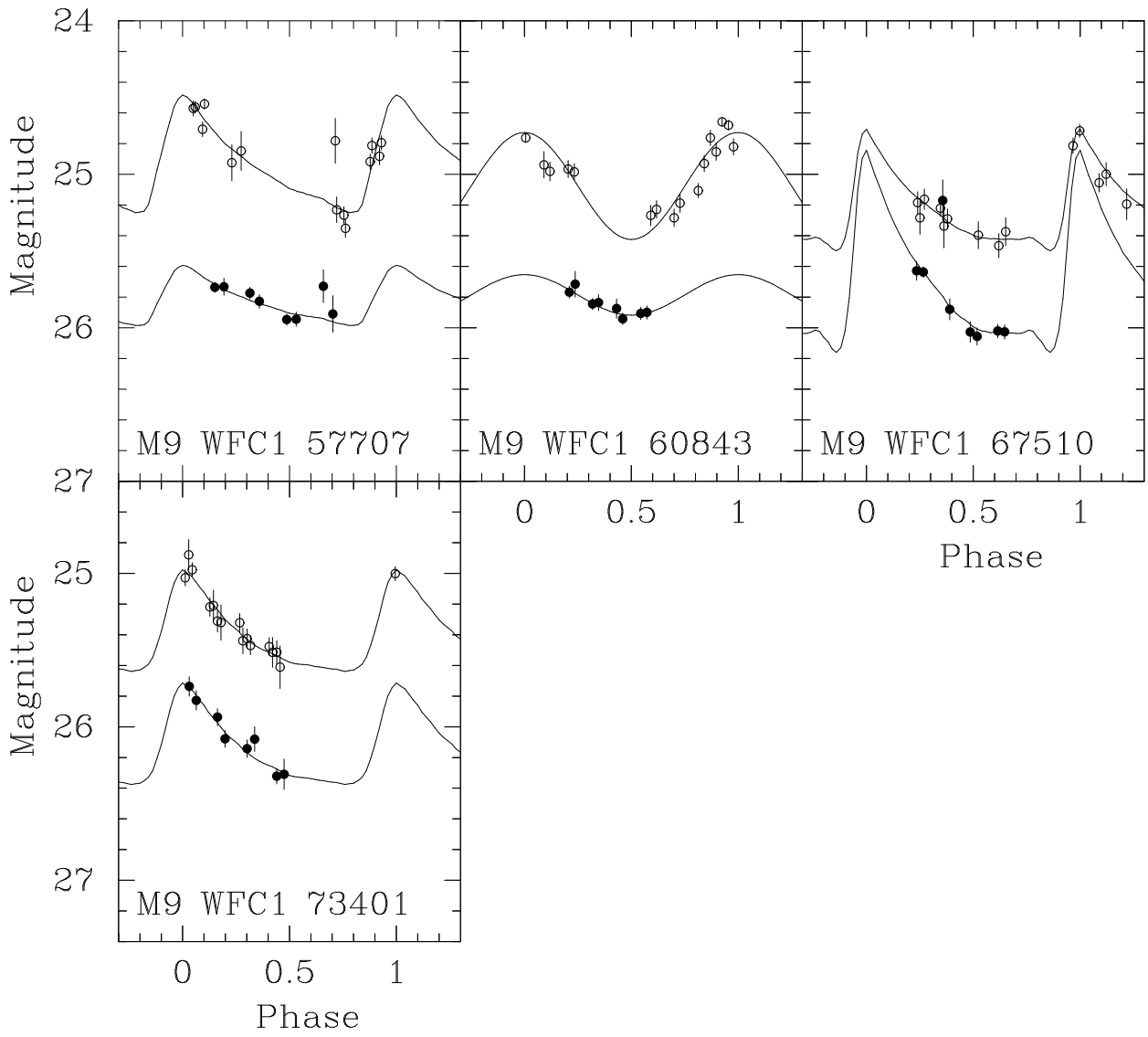


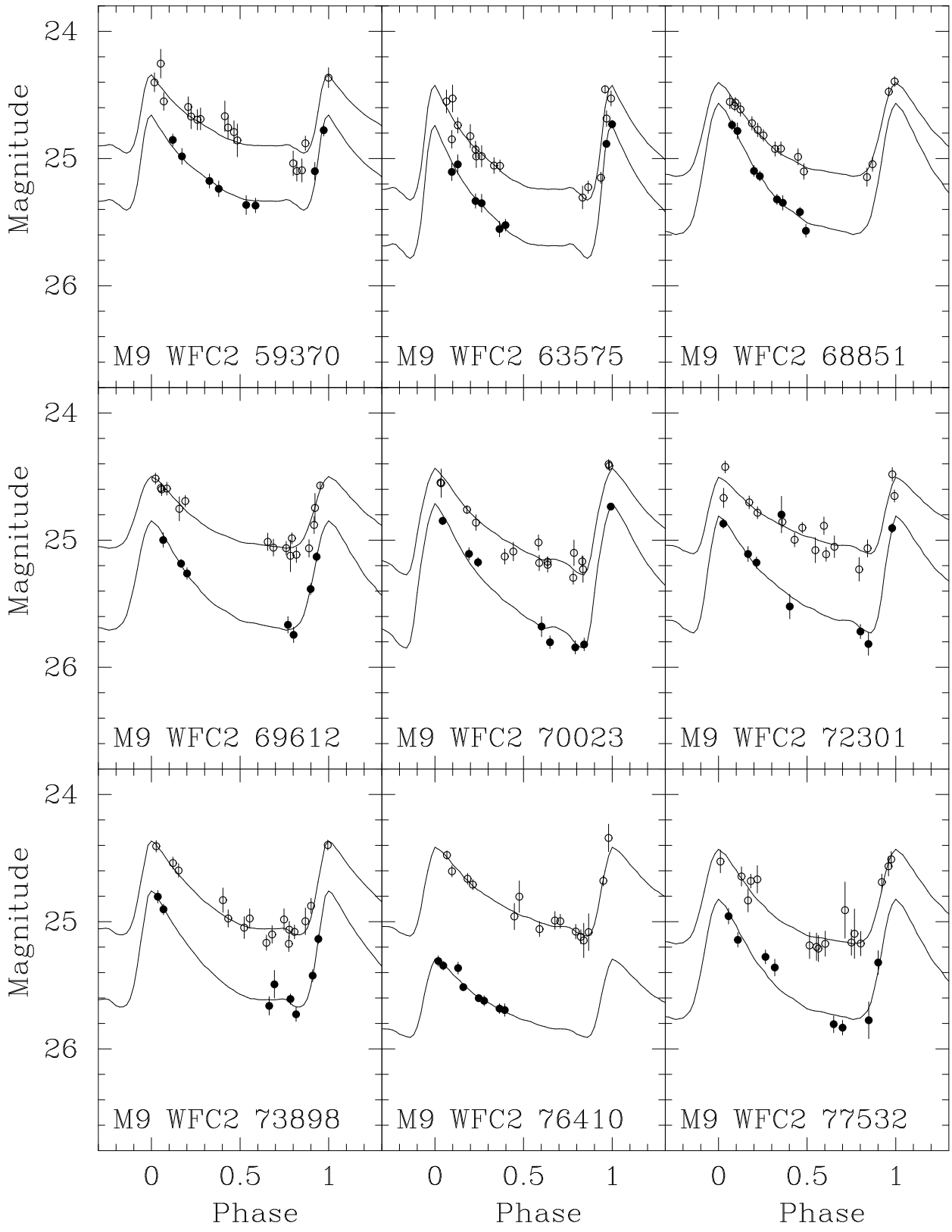


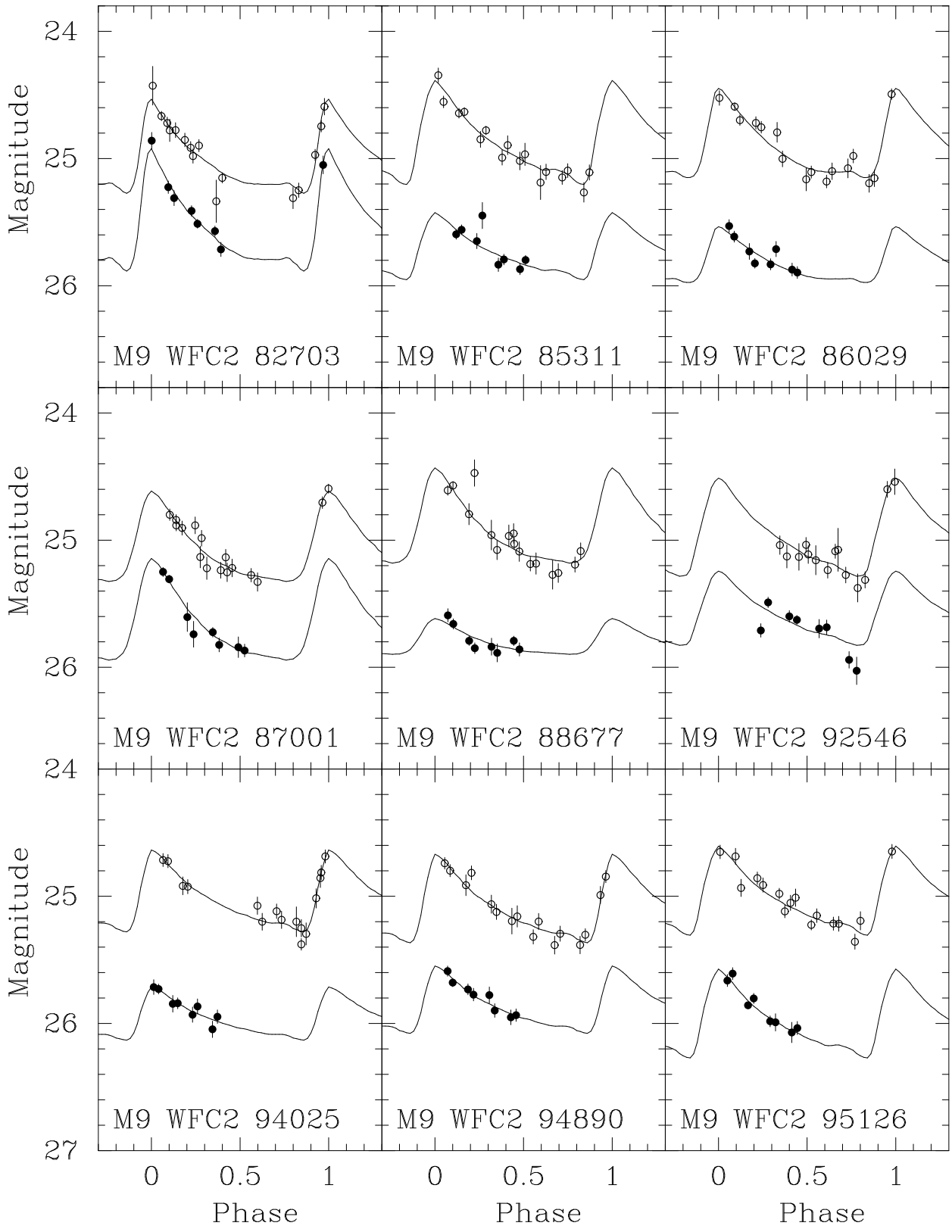


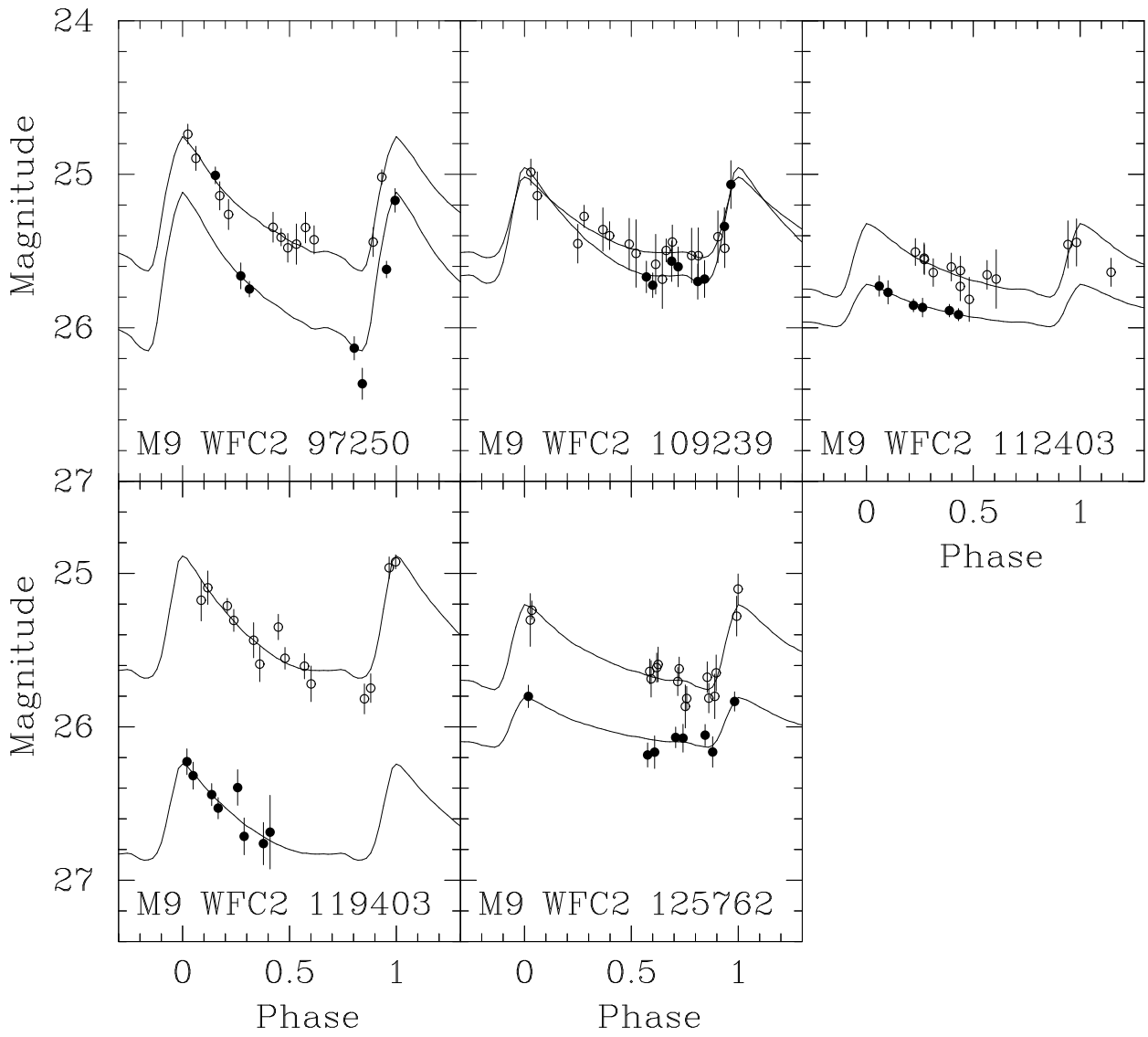












This figure "f12.jpg" is available in "jpg" format from:

<http://arxiv.org/ps/astro-ph/0605580v1>



